Politecnico di Torino

Master's Degree in Physics of Complex Systems

Politecnico
di Torino

Master's Thesis

Non-reciprocal interactions in flocking models

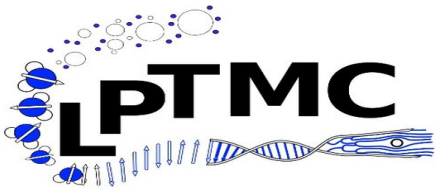

Supervisors:
Alessandro Pelizzola
Alexandre Solon

Candidate:
Daniele Carichini

March 2025

Contents

1 Introduction **1**
- 1.1 Active Matter and Collective Dynamics 1
- 1.2 The Vicsek Model 3
  - 1.2.1 Flocking Transition 4
  - 1.2.2 Phase Diagram and Micro-phase Separation 5
- 1.3 Continuous Theory for the Vicsek Model 7
  - 1.3.1 The Toner-Tu Hydrodynamic Equations 7
  - 1.3.2 Generalized Vicsek Model 8
  - 1.3.3 Boltzmann-Ginzburg-Landau Approach 9

2 Study of a Non-reciprocal Vicsek Model **15**
- 2.1 Description of the Model 15
- 2.2 Emergence of Smectic Order 17
- 2.3 Phase Diagram Analysis 18
  - 2.3.1 Smectic Order Parameter 18
  - 2.3.2 Phase Diagram and Finite Size Scaling of Smectic Order 20
- 2.4 Chiral Simmetry Breaking 22

3 Conclusions **26**

A Active Ising Model **27**

B Boltzmann Equation for Polar Vicsek Particles **29**

Abstract

Active matter is a field within out-of-equilibrium statistical physics that studies systems at the microscopic scale capable of converting ambient energy into self-propulsion or other forms of mechanical motion. The Vicsek model (VM), which describes the transition to collective motion in self-propelled particles, serves as a paradigmatic example in this discipline. Known for its simplicity and numerical tractability, the VM effectively captures the onset of flocking behavior. While fundamental forces must obey Newton's action-reaction principle, effective descriptions of active matter systems often involve reciprocity-breaking interactions, especially at the mesoscopic level, where such interactions may be more the rule than the exception. A striking consequence of non-reciprocal (NR) interactions in two-species systems is the emergence of chiral phases. This raises the question of whether chiral phases, or other forms of chirality, can emerge in one-species NR active models. Prior work on active smectics introduced variants of the Vicsek model incorporating pairwise non-reciprocal repulsion and noted the spontaneous emergence of global rotation. In this study, a numerical investigation of chirality-breaking mechanisms in the non-reciprocal Vicsek model is presented, aiming to explore the potential role of NR interactions in the emergence of chiral phases. To this end, a smectic order parameter is introduced as a numerical tool to analyze rotational dynamics. The dependence on non-reciprocal repulsion strength is then quantified through an exponential fit of the angular velocity autocorrelation function.

Chapter 1

Introduction

1.1 Active Matter and Collective Dynamics

Nonequilibrium systems manifest in a broad range of scenarios, each exhibiting unique behaviors. However, they can often be categorized based on shared features [5]. One such category consists of systems that are relaxing toward thermal equilibrium but have not yet fully reached it. This relaxation can proceed relatively smoothly or, in some cases, become exceedingly slow, as observed in glassy systems. Despite differences in the relaxation process, there is always a distinct direction in which the system evolves or would evolve if not obstructed.

Another class of nonequilibrium systems includes those that are unable to reach equilibrium due to external constraints that sustain a continuous flow of energy or matter. A common example is a heat conduction experiment, where a material is placed between two reservoirs maintained at different temperatures, generating a persistent thermal current.

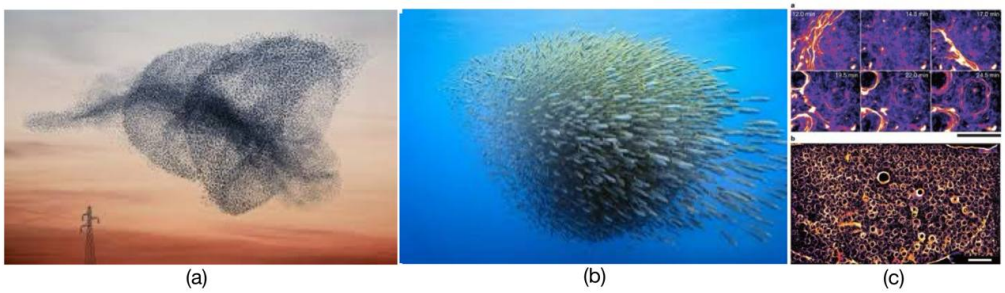

Figure 1.1: Examples of collective phenomena: (a) flock of birds, (b) school of fish, (c) Emergence of vortices of microtubules [21].

A third category is active matter, which consists of systems that dissipate energy on a microscopic scale, resulting in irreversible dynamics. In these systems, self-propelled particles draw energy from an internal or ex-

ternal source and convert it into directed motion, thereby maintaining a perpetual nonequilibrium state. Unlike systems that passively relax toward equilibrium or those influenced by boundary conditions, active matter inherently breaks time-reversal symmetry because each particle persistently dissipates energy. What makes this category particularly intriguing is the emergence of complex collective behaviors in many-body interactions.

Active matter encompasses a diverse array of self-propelled systems, including biological examples such as flocks of birds [2], schools of fish[25], actin filaments [17], and microtubules in motility assays [21], as well as synthetic examples like autophoretic colloids [22, 4, 13]. The study of active matter has contributed to the development of theoretical models that capture the fundamental interactions governing these behaviors. For example, two widely studied models for active particles are the Run-and-Tumble Particle (Figure 1.2(a)) and the Active Brownian Particle (Figure 1.2(b)).

The Run-and-Tumble Particle alternates between two phases:

- Run: The particle moves in a straight line with constant velocity.
- Tumble: At random intervals, the particle abruptly changes direction before initiating a new run.

In contrast, the Active Brownian Particle moves at a constant speed but undergoes gradual directional changes due to random rotational diffusion, resulting in a smoother trajectory rather than abrupt reorientations.

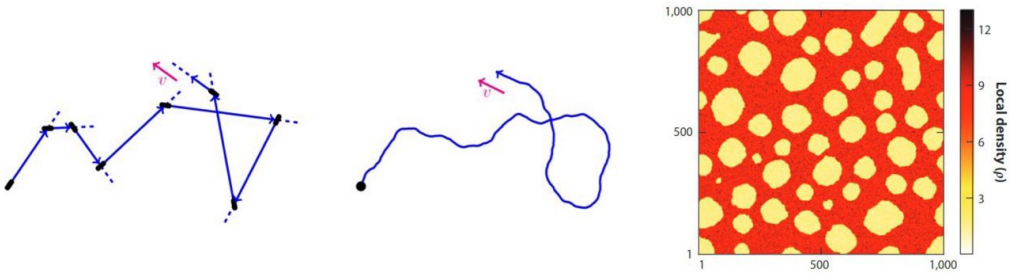

Figure 1.2: (a)-(b) Visualization of the dynamics of run-and-tumble and active brownian particles. (c) Two-dimensional run-and-tumble system undergoing motility-induced phase separation from [5].

Active matter models can be further classified into scalar and aligning, based on whether the particles interact by adjusting their orientation in response to their neighbors:

- Scalar active matter consists of particles that do not align with one another but instead interact through steric or other non-orientational

forces. A particularly notable phenomenon in this class, which has no direct equilibrium counterpart, is Motility-Induced Phase Separation (MIPS). In MIPS, particles spontaneously segregate into dense "liquid-like" clusters surrounded by a dilute "gas-like" phase, where movement is freer. This behavior can be reproduced using minimal models of Active Brownian Particles or Run-and-Tumble Particles interacting via steric repulsion. Intuitively, MIPS arises because particle collisions slow movement in dense areas, causing further accumulation and creating a self-reinforcing feedback loop.

- Aligning active matter, on the other hand, consists of particles that actively adjust their orientation based on local interactions. A foundational model in this category is the Vicsek model, introduced in 1995 by Vicsek and collaborators [24]. This model has been highly influential in active matter research. In its original form, it describes point-like self-propelled particles moving at a constant speed within a two-dimensional periodic domain. The particles follow local alignment rules with an added angular noise term. A key feature of the Vicsek model is the spontaneous emergence of collective motion: when noise levels are sufficiently low, a large number of individuals synchronize their movement, forming a coherently moving cluster. A more detailed and generalized version of this model will be introduced in the next section.

1.2 The Vicsek Model

In the Vicsek model [24], point particles move at constant speed v_0, adjusting their direction of motion to that of the average velocity of their neighbors, up to some noise term accounting for external or internal perturbations. For a finite density of particles in a finite box, perfect alignment is reached easily in the absence of noise: in this fluctuation-less collective motion, the macroscopic velocity equals the microscopic one. On the other hand, for strong noise particles are essentially non-interacting random walkers and their macroscopic velocity is zero, up to statistical fluctuations.
Vicsek et al. showed that the onset of collective motion occurs at a finite noise level. In other words, there exists, in the asymptotic limit, a fluctuating phase where the macroscopic velocity of the total population is, on average, finite. Working mostly in two space dimensions, they concluded, on the basis of numerical simulations[9, 24], that the onset of this ordered motion is well described as a novel non-equilibrium phase transition leading to long range order, at odds with equilibrium where the continuous XY symmetry cannot be spontaneously broken in two space dimensions and below, due to Mermin-Wagner theorem.
Let us now introduce the dynamical rule defining the Vicsek model. Point

particles labeled by an integer index i move off-lattice in a space of dimension d(that in the following we will always consider to be 2) with a velocity v_i of fixed modulus v_0. The direction of motion of particle i depends on the average velocity of all particles (including i) in the spherical neighborhood of radius r_0 centered on i. The discrete-time dynamics is synchronous: the direction of motion and the position of all particles are updated at each timestep Δt, in a driven, overdamped manner:

$$\vec{v}_i(t + \Delta t) = v_0 \cdot (\mathcal{R}_\eta \circ \mathcal{N}) \left[\sum_{j \in S_i} \vec{v}_j(t) \right] \tag{1.1}$$

where $\mathcal{N}$ is a normalization operator ($\mathcal{N}(\vec{w}) = \vec{w}/|\vec{w}|$) and $\mathcal{R}_\eta$ performs a random rotation uniformely distributed around the argument vector: in $d = 2$, $\mathcal{R}_\eta(\vec{v})$ is uniformely distributed around $\vec{v}$ inside an arc of amplitude $2\pi\eta$; in $d = 3$, it lies in the solid angle subtended by a spherical cap of amplitude $4\pi\eta$ and centered around $\vec{v}$. The particles' positions r_i are then simply updated by streaming along the chosen direction as in:

$$\vec{r}_i(t + \Delta t) = \vec{r}_i(t) + \Delta t \cdot \vec{v}_i(t + \Delta t) \tag{1.2}$$

1.2.1 Flocking Transition

In the following, we present some numerical results on the above introduced model. The natural order parameter for our polar particles is simply the macroscopic mean velocity, conveniently normalized by the microscopic velocity v_0:

$$\vec{\varphi}(t) = \frac{1}{v_0} \langle \vec{v}_i(t) \rangle_i$$

where $\langle \cdot \rangle_i$ stands for the average over the whole population. We will be interested in the scalar order parameter given by the modulus of of the mean velocity $\varphi(t) = |\vec{\varphi}(t)|$. In the following we set, without loss of generality, $\Delta t = 1$ and $r_0 = 1$, and express all time and length scales in terms of these units. Fixing the microscopic velocity to a specific value ($v_0 = 0.5$ for the results below), we remain with two main parameters: the noise amplitude η and the global density of particles ρ_0.

In early numerical studies [9][24] the onset of collective motion was found to be a novel continuous phase transition spontaneously breaking rotational symmetry. However, it was later shown in [10] that beyond the typical sizes originally considered, the discontinuous nature of the transition emerges. This result is reproduced in figure 1.3.

Another sign of the emergence of the discontinuity in the transition is given by the Binder cumulant [6]:

$$G(\eta, L) = 1 - \frac{\langle \varphi^4 \rangle_t}{3 \langle \varphi^2 \rangle_t^2}$$

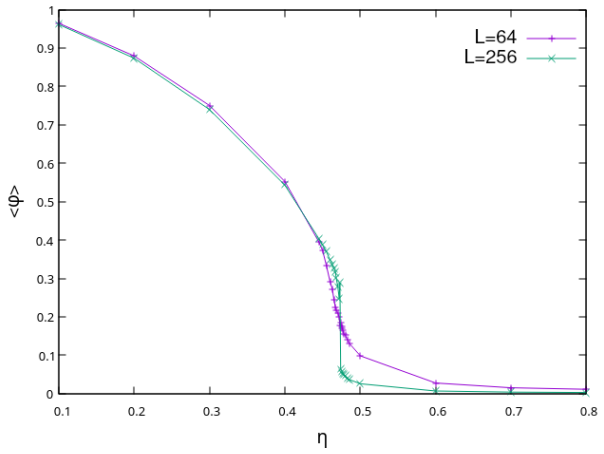

Figure 1.3: Transition to collective motion for two different system sizes. The discontinuous nature of the transition arises only for the larger system.

Indeed, at a first-order phase transition point, the Binder cumulant exhibits a sharp drop towards negative values, while varying continuously at a second-order one. The two mentioned behaviors are shown in figure 1.4.

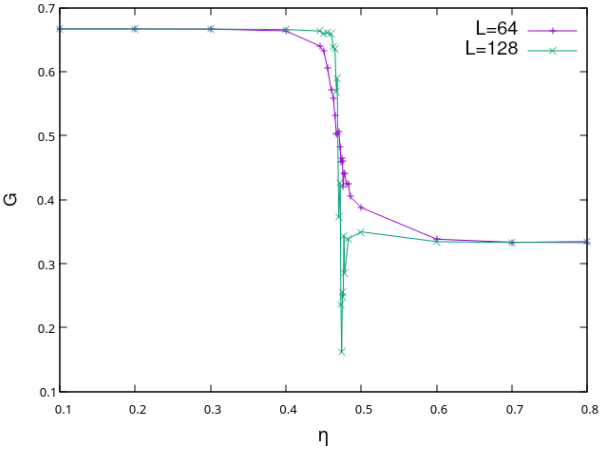

Figure 1.4: Change of the behavior of the Binder cumulant for higher system sizes, due to the emergence of the discontinuous nature of the flocking transition.

1.2.2 Phase Diagram and Micro-phase Separation

As mentioned earlier, the two main parameters controlling the system's behavior are the noise intensity η and the global density ρ_0. So far, we have analyzed how the system responds to increasing noise at a fixed density. However, one can explore the full (ρ_0, η) phase space and observe that at

high noise levels or low densities, the system remains in a disordered state, where particles move randomly with no global coordination. In contrast, at low noise and sufficiently high densities, the system undergoes a first-order transition to an ordered phase, where particles spontaneously align, resulting in large-scale collective motion.

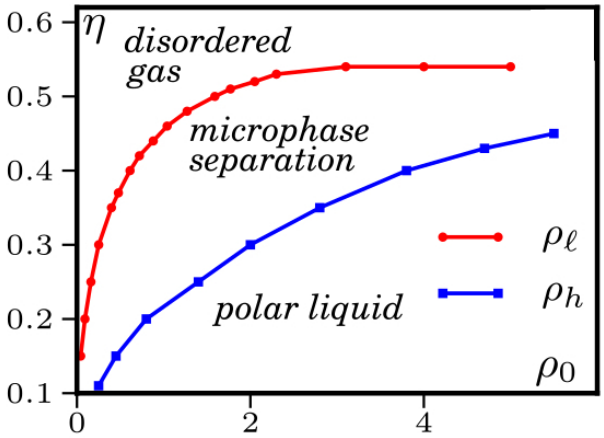

Figure 1.5: Phase diagram of the Vicsek model from [20]. The curves $\rho_h(\eta)$ and $\rho_l(\eta)$ mark the limit of the coexistence region.

At very low densities, the system stays disordered regardless of noise because there are too few interactions to sustain collective motion. As density increases, the critical noise η_c required to destroy order also increases, defining a clear phase boundary in the (ρ_0, η) plane. Near this transition, the system exhibits a coexistence of ordered and disordered regions, where high-density, ordered traveling bands emerge and move through a disordered background. This behavior resembles a liquid-gas transition: the ordered (flocking) phase acts like a dense liquid, while the disordered phase behaves like a gas. The (ρ_0, η) phase diagram is shown in Figure 1.5.

The arrangement of the ordered phase into traveling bands within the coexistence region is known as microphase separation. This phenomenon is a distinct feature of the Vicsek model and is not a general property of flocking transitions. For instance, the active Ising model (Appendix A), despite also displaying a coexistence region, does not exhibit microphase separation. This difference has been investigated using continuum theories [20], but a full analytical understanding is still lacking.

Within the coexistence region, increasing the density leads to the formation of more bands, while their width remains constant. Bands can be detected by analyzing the density or the order parameter averaged along the direction perpendicular to their motion (which coincides with the direction of polar order). In the presence of bands, both $\langle\rho\rangle_\perp$ and $\langle\varphi\rangle_\perp$ exhibit distinct peaks, as illustrated in Figure 1.6.

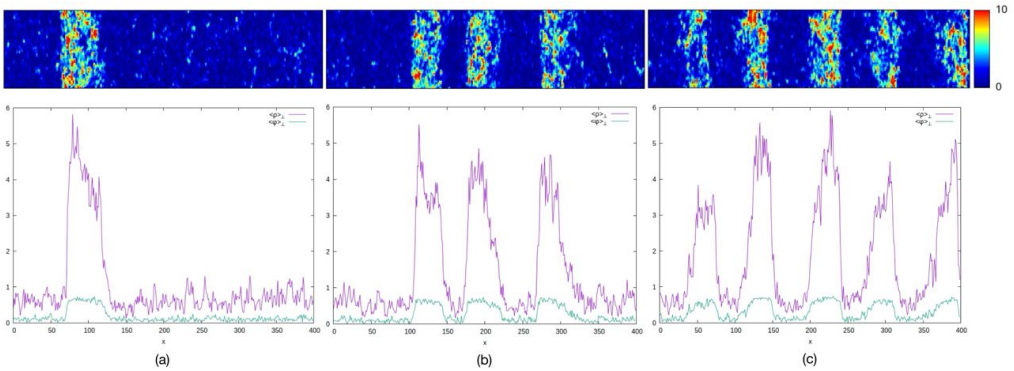

Figure 1.6: Configurations with increasing values of $\rho_0(1.05, 1.45, 1.95$, respectively for (a),(b),(c)). The number of bands increase with the mean density of the system. For each configuration is shown the plot of both $\langle\rho\rangle_\perp$ and $\langle\varphi\rangle_\perp$ exhibiting peaks in corrispondence of the position of the bands. Other parameters of the model are fixed: $L_x = 400$, $L_y = 50$, $\eta = 0.4$, $v_0 = 0.5$.

1.3 Continuous Theory for the Vicsek Model

Understanding collective motion in active systems requires models that go beyond particle-based simulations. While microscopic models provide detailed insights, they often become computationally expensive and difficult to analyze at large scales. A more effective approach is to describe the system using continuum theories, which capture the macroscopic behavior of the system through a set of coarse-grained equations.

1.3.1 The Toner-Tu Hydrodynamic Equations

The first continuous theory for the Vicsek model where developed by Toner and Tu[23]. In this framework, the system is described by two main fields: the density $\rho(\vec{r}, t)$ and the velocity $v(\vec{r}, t)$, which evolve according to a set of nonlinear partial differential equations built phenomenologically, considering all the terms allowed by rotational symmetry. These equations, account for both the spontaneous emergence of order and the fluctuations that govern large-scale dynamics. In their most general form the PDEs are:

$$\partial_t\rho + \nabla\cdot(\rho\vec{v}) = 0 \tag{1.3}$$

$$\partial_t\vec{v}+\lambda_1(\vec{v}\cdot\nabla)\vec{v}+\lambda_2(\nabla\cdot\vec{v})\vec{v}+\lambda_3\nabla|\vec{v}|^2 = D\nabla^2\vec{v}+\nu_b\nabla(\nabla\cdot\vec{v})+(r-u|\vec{v}|^2)\vec{v}+ \\ -\nabla P(\rho)+\vec{\eta} \tag{1.4}$$

The first equation represents mass conservation, while the second describes the evolution of the velocity field, including several terms each representing:

- Advection: $\lambda_1(\vec{v}\cdot\nabla)\vec{v} + \lambda_2(\nabla\cdot\vec{v})\vec{v} + \lambda_3\nabla|\vec{v}|^2$
- Viscosity: $D\nabla^2\vec{v}$
- Bulk viscosity: $\nu_b\nabla(\nabla\cdot\vec{v})$
- Aligning: $(r - u|\vec{v}|^2)\vec{v}$
- Pressure $-\nabla P(\rho)$
- Noise: $\vec{\eta}$

And can be thought as a Navier-Stokes equation plus an aligning Ginzburg-Landau term.

A key prediction of the Toner-Tu theory is that long-range order can persist in two dimensions, defying the expectations from equilibrium systems, where the Mermin-Wagner theorem would forbid such ordering. The theory also predicts phase coexistence between ordered and disordered regions.

1.3.2 Generalized Vicsek Model

A significant limitation inherent to the Toner-Tu framework lies in its disconnection from the parameters governing the microscopic level of the system. Without the connection between the parameters of the Vicsek model and the coefficients present in the Toner-Tu equations, constructing phase diagrams that correspond to those obtained from microscopic models or experimental studies becomes difficult. Therefore, the reliability and representational power of hydrodynamic equations cannot be rigorously evaluated.

For this reason, methodologies have been developed to begin with a specific microscopic model and derive the corresponding hydrodynamic equations, establishing a link between microscopic parameters and hydrodynamic transport coefficients. Although exact derivations are currently confined to a narrow subset of microscopic models, alternative methods rely on constructing an intermediate kinetic-level description before proceeding to derive hydrodynamic equations from it.

In the following we will introduce a more general formulation of the Vicsek model, more suitable to the development of a kinetic description[15].

Particles are described by their position $\vec{r}$ and a unit vector defined by $\theta \in [-\pi, +\pi]$. The update rule is the same of 1.2. However, we consider

$\vec{v}$ as a random vector drawn from a displacement distribution $\phi(v, \theta_v - \theta)$, θ_v being the angle defining the orientation of $\vec{v}$. Note that the numerical model is recovered in the case $\phi(v, \theta_v - \theta) = \delta(v - v_0)\delta(\theta_v - \theta)$.
The heading angle of a particle θ evolves according to the stochastic dynamics given by:

$$\theta' = \psi^{(p)}(\theta, \theta_{i_1}, ..., \theta_{i_p}) + \delta\theta$$

Where $\delta\theta$ is an angle drawn from a symmetrically distributed random distribution P_η and $\psi^{(p)}$ is the interaction rule for the p-neighbours case. When no neighbours are present, particles simply experience self-diffusion events $\psi^{(0)}(\theta) = \theta + \eta$.
Before entering the continuous theory, let us consider the two-body interaction rule $\psi(\theta_1, \theta_2)$. We are still considering isotropic interactions, this impose that for an arbitrary rotation of angle α:

$$\psi(\theta_1 + \alpha, \theta_2 + \alpha) = \psi(\theta_1, \theta_2) + \alpha \mod (2\pi)$$

Choosing $\alpha = -\theta_1$, we find that the two-body interaction rule is determined by a function only of the angles difference:

$$\psi(\theta, \theta + \Delta) = \theta + H(\Delta)$$

1.3.3 Boltzmann-Ginzburg-Landau Approach

For most systems similar to the Vicsek model, kinetic equations are formulated to govern the one-body probability distribution function $f(\vec{r}, \theta, t)$. This function describes the likelihood of finding particles at a specific position $\vec{r}$, heading the direction defined by θ, at time t. Deriving such an equation necessitates factorizing a multi-body distribution function into a product of one-body functions, a step justified under the strong "molecular chaos" assumption. This assumption posits that the orientations of the particles become decorrelated between successive interactions. However, the molecular chaos hypothesis is particularly stringent: particles that have just interacted often remain aligned for a significant duration, preserving correlations. Consequently, quantitative agreement between kinetic-level descriptions and microscopic models is often not obtained.

Moreover, additional assumptions are required to derive hydrodynamic equations from kinetic ones. As a result, hydrodynamic theories should realistically aim to provide qualitative, or at best semi-quantitative, consistency with the underlying microscopic dynamics.

Here we focus on the approach pioneered and developed by Eric Bertin and his collaborators [3, 15], referred to as the Boltzmann-Ginzburg-Landau (BGL) framework.

The BGL approach is particularly suited for systems like the Vicsek model and serves as a robust methodology for deriving hydrodynamic equations. To illustrate this, we will apply the BGL framework directly to the

generalized Vicsek model. The derivation begins by formulating a Boltzmann equation, a step that formally requires the assumption of particle diluteness. The generalized Boltzmann equation for polar Vicsek particles can be expressed as follows (a full derivation is provided in Appendix B):

$$\partial_t f(\vec{r},\theta,t)+v_0 n_\alpha(\theta)\partial_\alpha f(\vec{r},\theta,t) = D_0\delta_{\alpha\beta}\partial_\alpha\partial_\beta f(\vec{r},\theta,t)+D_1 q_{\alpha\beta}\partial_\alpha\partial_\beta f(\vec{r},\theta,t)+ \\ + I_{sd}[f] + I_{col}[f] \quad (1.5)$$

Where $\hat{n}(\theta)$ is the unit vector pointing in the direction θ, D_0 and D_1 are the isotropic and anisotropic diffusion coefficients proportional, respectively, to the identity $\delta_{\alpha\beta}$ and the nematic tensor $q_{\alpha\beta}(\theta) = n_\alpha(\theta)n_\beta(\theta) - \frac{1}{2}\delta_{\alpha\beta}$. It can be shown that the coefficients are expressed by:

$$D_0 = \frac{1}{4}\big(\langle v^2\rangle - v_0^2\big)\Delta t \quad (1.6)$$

$$D_1 = \frac{1}{2}\big(\langle v^2\cos 2\delta\theta\rangle - v_0^2\big)\Delta t \quad (1.7)$$

Note that both vanish for the case that we studied numerically, for which we do not have diffusion in the positional part of the dynamics $\big(\phi = \delta(v - v_0)\delta(\theta_v - \theta)\big)$. Regarding the other terms, we have the integrals describing the dynamics of the heading angle θ:

$$I_{sd}[f] = -\lambda f(\vec{r},\theta,t) + \lambda\int_0^{2\pi} d\theta' f(\vec{r},\theta',t)P_\eta(\theta-\theta') \quad (1.8)$$

$$I_{col}[f] = -2r_0v_0 f(\vec{r},\theta,t)\int_0^{2\pi} d\theta' K(\theta'-\theta)f(\vec{r},\theta,t)+ \quad (1.9)$$

$$+ 2r_0v_0\int_0^{2\pi} d\theta_1\int_0^{2\pi} d\theta_2 K(\theta_2-\theta_1)f(\vec{r},\theta_1,t)f(\vec{r},\theta_2,t)P_\eta\big(\theta-\Psi(\theta_1,\theta_2)\big)$$

Which describe self-diffusion and two-body collision events, respectively. λ is the rate for self-diffusion events, while $K(\Delta)$ is the collision kernel and it depends only on the angle difference, to respect the symmetry of the system. Since we are considering polar particles, it holds $K(\Delta) = 2\big|\sin\big(\frac{\Delta}{2}\big)\big|$. We can make the Boltzmann equation dimensionless by rescaling appropriately the quantities:

$$t \to \lambda^{-1}t\,,$$
$$\partial_{x,y} \to \lambda v_0^{-1}\partial_{x,y}\,,$$
$$f(\vec{r},\theta,t) \to \rho_0 f(\vec{r},\theta,t).$$

In such way, we ramain with only two control parameters: the variance η^2 of the noise distribution and the dimensionless density $\tilde{\rho}_0 \doteq 2r_0v_0\rho_0\lambda^{-1}$.

The next step is to exploit the periodicity of the angular part of the single-particle distribution $f(\vec{r},\theta,t)$, expanding it in terms of angular Fourier modes:

$$f(\vec{r},\theta,t) = \frac{1}{2\pi}\sum_{k=-\infty}^{+\infty} f_k(\vec{r},t)\, e^{-ik\theta} \tag{1.10}$$

Where

$$f_k(\vec{r},t) = \int_0^{2\pi} d\theta f(\vec{r},\theta,t) e^{ik\theta} \tag{1.11}$$

Being f a real-valued function, we will have $f_{-k}(\vec{r},t) = f_k^*(\vec{r},t)$. We observe also that when working near onset of orientational order we have smooth angular variations of $f(\vec{r},\theta,t)$, implying that the modes f_k quickly decay to zero for increasing values of k. This will be useful to obtain hydrodynamic equations, which has to be a closed set of equations for the first few modes, indeed the first three modes correspond, respectively, to the complex representation of density ρ, momentum $\vec{w} = \rho\vec{v}$ and nematic $\mathbf{S} = \rho\mathbf{Q}$ fields:

$$f_0(\vec{r},t) = \int_0^{2\pi} d\theta f(\vec{r},\theta,t) = \rho(\vec{r},t)\,, \tag{1.12}$$

$$f_1(\vec{r},t) = \int_0^{2\pi} d\theta f(\vec{r},\theta,t) e^{i\theta} \; = w_x(\vec{r},t) + i w_y(\vec{r},t), \tag{1.13}$$

$$f_2(\vec{r},t) = \int_0^{2\pi} d\theta f(\vec{r},\theta,t) e^{2i\theta} = 2[S_{xx}(\vec{r},t) + S_{xy}(\vec{r},t)]\,. \tag{1.14}$$

Now we will switch to the Fourier space in the Boltzmann equation 1.5, multiplying by $e^{ik\theta}$ and integrating over θ all members, this will result in an infinite hierarchy of PDEs governing the evolution of the modes f_k.
In the following, we will consider a class of systems for which it is not necessary to consider the angle diffusion dynamics($D_0 = D_1 = 0$) so those term will we discarded. Space and time dependencies of the functions will be implicit, to lighten the notation. Let us consider the terms one by one:

- Drift term:

  $$\hat{n}(\theta)\cdot\vec{\nabla} f(\theta) \longrightarrow \int_0^{2\pi} d\theta e^{ik\theta} \begin{pmatrix}\cos\theta\\ \sin\theta\end{pmatrix}\begin{pmatrix}\partial_x\\ \partial_y\end{pmatrix} f(\theta) = \frac{1}{2}(\nabla^* f_{k+1} + \nabla f_{k-1})$$

  Where we used the complex gradient $\nabla = \partial_x + i\partial_y$.

- Self-diffusion integral:

  $$I_{sd}[f] = -\lambda f(\vec{r},\theta,t) + \lambda\int_0^{2\pi} d\theta' f(\vec{r},\theta',t) P_\eta(\theta-\theta') \longrightarrow (P_k - 1) f_k$$

  Where P_k is the k^{th} mode of the distribution P_η, and we exploited the properties of the convolution product with respect to the Fourier transform.

- Collision integral: Let us consider just the gain contribution for the moment.

$$\int_0^{2\pi} d\theta e^{ik\theta} \int_0^{2\pi} d\theta_1 \int_0^{2\pi} d\theta_2 K(\theta_2-\theta_1) f(\theta_1) f(\theta_2) P\big[\theta - \theta_1 - H(\theta_2-\theta_1)\big]$$

Expanding P_η and $f(\theta_2)$ in Fourier modes and applying the change of variable $\theta_2 \to \Delta + \theta_1$:

$$\frac{1}{(2\pi)^2}\sum_{q,l} P_l f_q \int_0^{2\pi} d\theta e^{i(k-l)\theta} \int_0^{2\pi} d\theta_1 e^{i(l-q)\theta_1} f(\theta_1) \int_0^{2\pi} d\Delta K(\Delta) e^{i\left[-q\Delta + lH(\Delta)\right]} =$$

$$= \frac{1}{2\pi}\sum_{q,l} P_l f_q \delta_{k,l} f_{l-q} \int_0^{2\pi} d\Delta K(\Delta) e^{i\left[-q\Delta + lH(\Delta)\right]} =$$

$$= P_k \sum_q I_{k,q} f_q f_{k-q}$$

Where we have defined the mode coupling function:

$$I_{k,q} = \frac{1}{2\pi}\int_0^{2\pi} d\Delta K(\Delta) e^{i\left[-q\Delta + kH(\Delta)\right]}$$

The loss contribution can be computed similarly. Summing the two contributions the collision term can be written as:

$$\sum_q J_{k,q} f_q f_{k-q}$$

With $J_{k,q} = \tilde{\rho_0}(P_k I_{k,q} - I_{0,q})$.
To go further, we have to specify the function $H(\Delta)$ defining the interaction rule. Let us then consider the canonical Vicsek model, which describes polar particles interacting with a ferromagnetic interaction($H(\Delta) = \frac{\Delta}{2}$). For such system the node coupling function becomes:

$$I_{k,q} = \frac{1}{2\pi}\int_0^{2\pi} d\Delta\, 2\left|\sin\left(\frac{\Delta}{2}\right)\right| e^{i\left(\frac{1}{2}k-q\right)\Delta} = \begin{cases} \frac{4}{\pi}\frac{1-(k-2q)(-1)^q \sin\left(\frac{k\pi}{2}\right)}{1-(k-2q)^2} & \text{if } |k-2q| \neq 1 \\ \frac{2}{\pi} & \text{otherwise} \end{cases}$$

After collecting all the terms, we end up with the following hierarchy:

$$\partial_t f_k + \frac{1}{2}(\nabla^* f_{k+1} + \nabla f_{k-1}) = (P_k - 1) f_k + \sum_q J_{k,q} f_q f_{k-q} \qquad (1.15)$$

The above system of equations admits the trivial disordered solution:

$$f_0 = \rho = 1\ ,\ f_k = 0\ \forall k > 0$$

The linear stability for this solution with respect to space-independent perturbations is given by:

$$\partial_t \delta f_k = [P_k - 1 + J_{k,0} + J_{k,k}]\delta f_k = \mu_k \delta f_k \tag{1.16}$$

Where we have introduced the linear coefficients $\mu_k[\rho] = P_k - 1 + J_{k,0} + J_{k,k}$, which as one can deduce from 1.16 determine the stability of the disordered solution (guaranteed only if $\mu_k < 0 \, \forall k$). For the scaling analysis that we are about to do, it is useful to write explicitly the first equations of the hierarchy:

$$\begin{aligned}
\partial_t \rho &= -\Re(\nabla^* f_1) \, , \\
\partial_t f_1 &= -\frac{1}{2}(\nabla^* f_2 + \nabla \rho) + \mu[\rho] f_1 + (J_{1,2} + J_{1,-1}) f_1^* f_2 + \dots \, , \\
\partial_t f_2 &= -\frac{1}{2}(\nabla^* f_3 + \nabla f_1) + \mu_2[\rho] + J_{2,1} f_1^2 + \dots \, , \\
&\vdots \\
\partial_t f_k &= -\frac{1}{2}(\nabla^* f_{k+1} + \nabla f_{k-1}) + \mu_k[\rho] f_k + (J_{k,1} + J_{k,k-1}) f_1 f_{k-1} + \dots \, , \\
&\vdots
\end{aligned} \tag{1.17}$$

Now, it can be shown that only $\mu_1 = P_1 - 1 + \frac{4}{\pi}(P_1 - \frac{2}{3})\rho_0$ can become positive at low noises and large densities. We can visualize a schematic phase diagram in figure 1.7. The line defined by $\mu_1 = 0$ in the (ρ_0, η) plane delimits the theoretical change of stability of the disordered solution. Below that line, the polar order $|f_1|$ grows and close to the transition we can thus assume that $|f_1| \approx \epsilon$ with $\epsilon \ll 1$. Using this information, we can see from 1.17 that each $k > 1$ mode takes non-zero value due to its non-linear coupling with mode f_1. This value is however kept small thanks to the negative coefficients $\mu_{k>1}$, we thus have $|f_2| \approx |f_1|^2 \, , \dots , |f_k| \approx |f_1 f_{k-1}| \, \forall k$. Moreover, the first equation of the hierarchy, which is simply a continuity equation, imposes $|\partial_t \rho| \approx |\nabla^* f_1|$, while the pressure in the polar field equation $(k+1)$ gives $|\partial_t f_1 \approx |\nabla \rho|$. Therefore, $|\delta\rho| = |\rho - \rho_0| = |\rho - 1| \approx |f_1| \approx \epsilon$ and $\partial_t \approx \nabla \approx \epsilon^\alpha$. The exponent is finally determined balancing in the polar field equation the terms $f_1^* f_2$ and $\nabla^* f_2$, resulting in $\alpha = 1$.

Thus, there is a unique scaling ansatz that allows one to attribute an ϵ order to each term of the hierarchy. Keeping terms up to second order, we can remove all equations of the hierarchy up to $k = 2$. Moreover, the equation for the nematic field reduces to:

$$f_2 = \frac{1}{\mu_2}\left[\frac{1}{2}\nabla f_1 - J_{2,1} f_1^2\right]$$

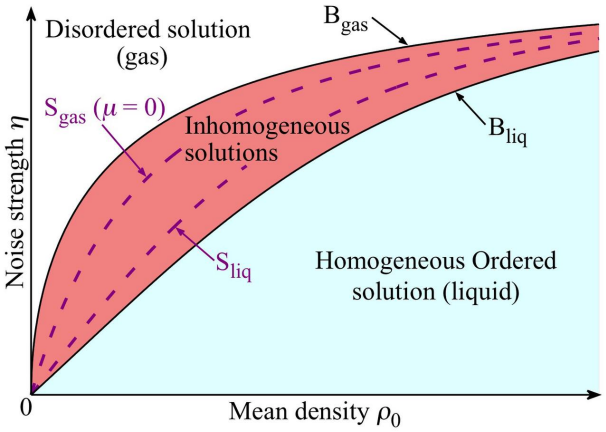

Figure 1.7: Schematic phase diagram from [7] of the hydrodynamic equations derived using the BGL method in the (ρ_0, η) plane. The S_{gas} line marks the (lower) limit of stability of the disordered solution and is defined by $\mu_1 = 0$. The S_{liq} line marks the (upper) limit of stability of the homogeneous ordered solution. The outermost lines (B_{gas} and B_{liq}) are the binodal lines. They mark the limit of existence of inhomogeneous band solutions.

Replacing f_2 by the above expression in the f_1 equation we finally get the closed hydrodynamic equations that we were looking for:

$$\begin{aligned} \partial_t \rho &= -\Re(\nabla^* f_1) \,, \\ \partial_t f_1 &= -\frac{1}{2}\nabla\rho + (\mu[\rho] + \xi|f_1|^2) f_1 + \nu\Delta f_1 - k_1 f_1 \nabla^* f_1 - k_2 f_1^* \nabla f_1 \,, \end{aligned} \tag{1.18}$$

With

$$\mu_1[\rho] = P_1 - 1 + \frac{4}{\pi}\left(P_1 - \frac{2}{3}\right)\rho_0\rho \,, \qquad \mu_2 = P_2 - 1 - \frac{8}{15\pi}(7 + 5P_2)\rho_0 \,,$$

$$\xi = -\frac{16(5P_1 - 2)(3P_2 + 1)\rho_0^2}{15\pi^2\mu_2} \,, \qquad \nu = -\frac{1}{4\mu_2} \,,$$

$$k_1 = -\frac{4(1 + 3P_2)\rho_0}{3\pi\mu_2} \,, \qquad k_2 = \frac{2(5P_1 - 2)\rho_0}{5\pi\mu_2} \,.$$

Chapter 2

Study of a Non-reciprocal Vicsek Model

We have already introduced the concept of active matter, where time-reversal symmetry is broken at the microscopic level by the continuous conversion of energy in self-propulsion. The most interesting part of this field comes when interactions are introduced: considering free single-particle dynamics does not bring much new physics with respect to its equilibrium counterpart. Thus, the interesting non-equilibrium features of active particles are displayed only when we make them interact with each other or the environment. We have seen, as an example, the emergence of collective motion in aligning active matter with the minimal Vicsek model.

While at the elementary level interactions must respect Newton's action-reaction principle, effective descriptions of active matter, which treats mesoscopic scales, often include reciprocity-breaking interactions. Examples of such behavior include predator-prey and promoter-inhibitor systems [12], but also systems whose dynamics depend on information propagation as in crowds of social animals [11, 1, 14, 8]. It is not necessary to consider binary system to observe non-reciprocity to arise. Based on the studies proposed in [16], we will propose a numerical study of a Vicsek model in which non-reciprocity is introduced, bringing to a novel type of smectic order and a surprising emergence of chirality in a microscopically achiral model.

2.1 Description of the Model

As already anticipated, we will study the variant of the Vicsek model proposed in [16]. In the spirit of the original dynamics, particles will evolve in a two-dimensional domain with periodic boundary conditions under the

following update rules:

$$\vec{r}_i(t+1) = \vec{r}_i(t) + v_0 \hat{e}\big(\theta_i(t+1)\big) \tag{2.1}$$

$$\theta_i(t+1) = \arg\left[\vec{A}_i(t) + \beta \vec{R}_i(t)\right] + \sigma\chi_i(t) \tag{2.2}$$

Where $\hat{e}(\theta) = (\cos\theta, \sin\theta)^T$ and, again, we have expressed all time and length scales in terms of Δt and r_0, respectively.

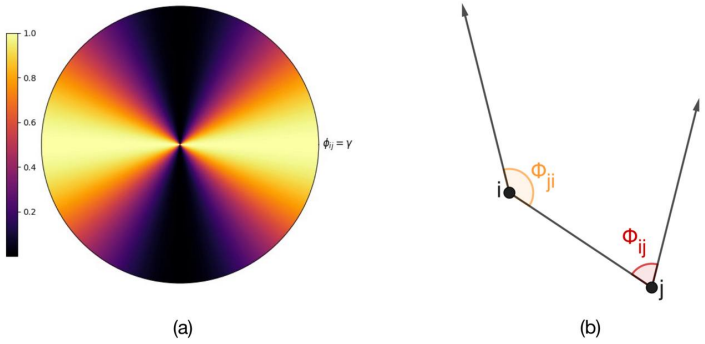

Figure 2.1: (a) Anisotropy of the interaction represented by the factor $\cos^2(\phi_{ji} - \gamma)$. (b) Schematic representation of the non-reciprocity generated by the lack of symmetry of ϕ_{ij} under indices exchange.

χ_i is an angular white noise uniformly distributed in $[-\frac{\pi}{2}, \frac{\pi}{2}]$, which makes the parameter σ the angular noise strength. The terms inside the arg function represent the attractive and repulsive interactions, respectively:

- $\vec{A}_i$ is the usual alignment term of the Vicsek model:

$$\vec{A}_i = \frac{1}{N_i} \sum_{i \sim j} \hat{e}(\theta_j)$$

- $\vec{R}_i$ is a repulsion, which can be chosen to be:

$$\vec{R}_i = \begin{cases} \frac{1}{N_i - 1} \sum_{j \sim i, j \neq i} \hat{r}_{ji} & \text{isotropic,} \\ \\ \frac{1}{N_i - 1} \sum_{j \sim i, j \neq i} \cos^2(\phi_{ji} - \gamma) \hat{r}_{ji} & \text{anisotropic.} \end{cases}$$

  Where $\hat{r}_{ji}$ is the unit vector pointing from j to i, and ϕ_{ji} is the angle between $\hat{r}_{ij}$ and $\vec{v}_i$.

Given the above definitions, it is clear that the role of β is the repulsion's strength, and together with the noise amplitude σ, they are the two main parameters of the model.

The fact that interactions are normalized by the number of neighbors N_i already introduces some non-reciprocity. In fact, even in the standard Vicsek model, Newton's third law is not strictly followed. However, the non-reciprocity in the repulsion has a bigger impact, as we will see. In the anisotropic case the explicit dependence on the angle ϕ_{ij} adds another layer of such non-reciprocity, as illustrated in figure 2.1.

2.2 Emergence of Smectic Order

In the following, we examine the collective dynamics of the system for three different types of repulsive forces: isotropic and anisotropic, with $\gamma = 0$ and $\gamma = \frac{\pi}{2}$.

Similar to the repulsion-free model, we observe an orientational order-disorder transition when σ increases or ρ_0 decreases. Our focus will be on how the system behaves as a function of σ and β, while keeping the remaining parameters fixed in accordance with [16] ($v_0 = 0.25$,$\rho_0 = 10$). At such high densities, the coexistence phase of the orientational order transition is practically absent.

The most significant effect of introducing repulsion is the emergence of smectic order in all the cases considered, provided σ and β take appropriate values. This smectic ordering becomes more stable at higher densities, which is why we have chosen to keep ρ_0 at a large fixed value.

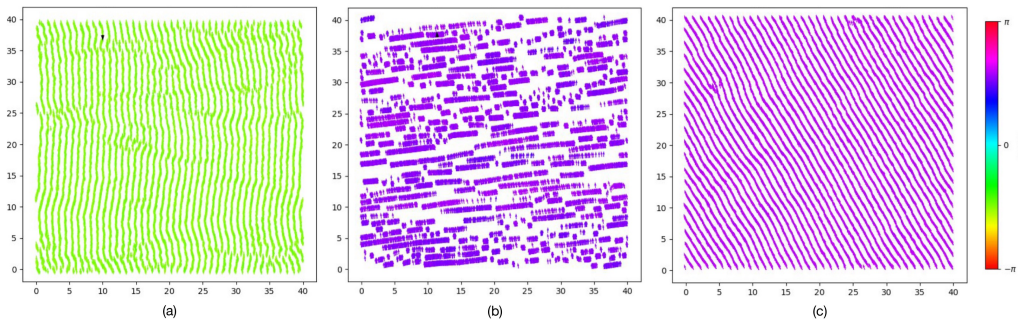

Figure 2.2: Emergence of smectic P order for isotropic(a) and anisotropic sides repulsion(c), and smectic A order for anisotropic front-and-back repulsion(b). Color indicates direction of particles.

The specific type of smectic order depends on the nature of the repulsive force. In the cases of isotropic repulsion and anisotropic repulsion with $\gamma = \frac{\pi}{2}$ (side repulsion), we observe a novel form of smectic order not found in equilibrium systems. In this newly identified phase, the particle axes align parallel to the layers, leading to what has been termed 'smectic P'. On the other hand, when anisotropic repulsion acts with $\gamma = 0$, the strongest repulsion occurs at the front and back of the particles, resulting in a smectic

A configuration. However, before reaching this final state, the system may undergo a long transient period where patches of smectic C order appear, forming local chevron-like structures due to competition between different smectic arrangements. Examples of all three cases are illustrated in Figure 2.2. The spacing between the smectic lines, as one could expect, is of the order of the interaction radius.

2.3 Phase Diagram Analysis

We have observed the emergence of smectic order in our models. To analyze this more quantitatively, we focus on the anisotropic model with $\gamma = \frac{\pi}{2}$, as this case is of particular interest for reasons that will become clear in the next section.

As an alternative to the conventional smectic order parameter, we propose a numerical approach that successfully reproduces a phase diagram consistent with the one reported in [16]. Finally, we conclude with a brief finite-size scaling analysis of the smectic order.

2.3.1 Smectic Order Parameter

Smectic order is typically quantified using the order parameters S_n, defined as:

$$S_n(t) = \frac{\langle |\rho(\vec{q}_n, t)|^2 \rangle_t}{N^2} \tag{2.3}$$

Where $\rho(\vec{q}_n, t)$ is the spatial Fourier transform of the density, computed at $\vec{q}_n = n\frac{2\pi}{a_l}\hat{z}$:

$$\rho(\vec{q}_n, t) = \int d^2 r \rho(\vec{r}, t) e^{-i\vec{q_n}\cdot\vec{r}} \tag{2.4}$$

Here, n is an integer, $a_l \approx r_0$ represents the layer spacing, and $\hat{z}$ is the direction normal to the smectic layers.

Although fast Fourier transform methods have been developed to compute S_n efficiently, Equation (2.3) can still be simplified to make the analysis of smectic order more practical and computationally accessible. To achieve this, we first recall the spatial correlation function:

$$g(\vec{r}) = \frac{\langle \rho(\vec{0})\rho(\vec{r}) \rangle}{\rho_0^2} \tag{2.5}$$

Focusing on the domain within a circle of radius $a \lesssim a_l$, we expect $g(\vec{r})$ to be nearly uniform for configurations that preserve translational symmetry, while exhibiting peaks at layer positions in smectic configurations.

Since our primary interest lies in the angular dependence, we integrate over the radial coordinate within this region, defining the angular correlation function:

$$G(\psi) = \int_0^a drrg(r, \psi) \tag{2.6}$$

Using the angular correlation function is advantageous because it can be directly computed via the empirical definition:

$$G(\psi) = \frac{1}{N} \sum_i \sum_{j \in C_a, j \neq i} \delta(\psi_{ij} - \psi) \tag{2.7}$$

where ψ_{ij} represents the angular position of particle j relative to particle i, and C_a denotes the set of particles within a circle of radius a centered in $\vec{r}_i$.

Figure 2.3 illustrates two examples of the typical profile of $G(\psi)$ for a uniform configuration and a smectic one. At this stage, we can extract smectic order information by quantifying how peaked $G(\psi)$ is around its maximum:

$$S = \left| \frac{\int_0^{2\pi} d\psi G(\psi) \cos(2(\psi - \psi^*))}{\int_0^{2\pi} d\psi G(\psi)} \right| \tag{2.8}$$

Where $\psi^* = \text{argmax}_{\psi \in [0, 2\pi)} G(\psi)$. As evident from Equation (2.8), S is bounded within the range $[0, 1]$, making it a good candidate to be the smectic order parameter.

In Figure 2.3, we also compare the angular correlation function of both configurations with $\cos(2(\psi - \psi^*))$, illustrating how S effectively captures smectic order information.

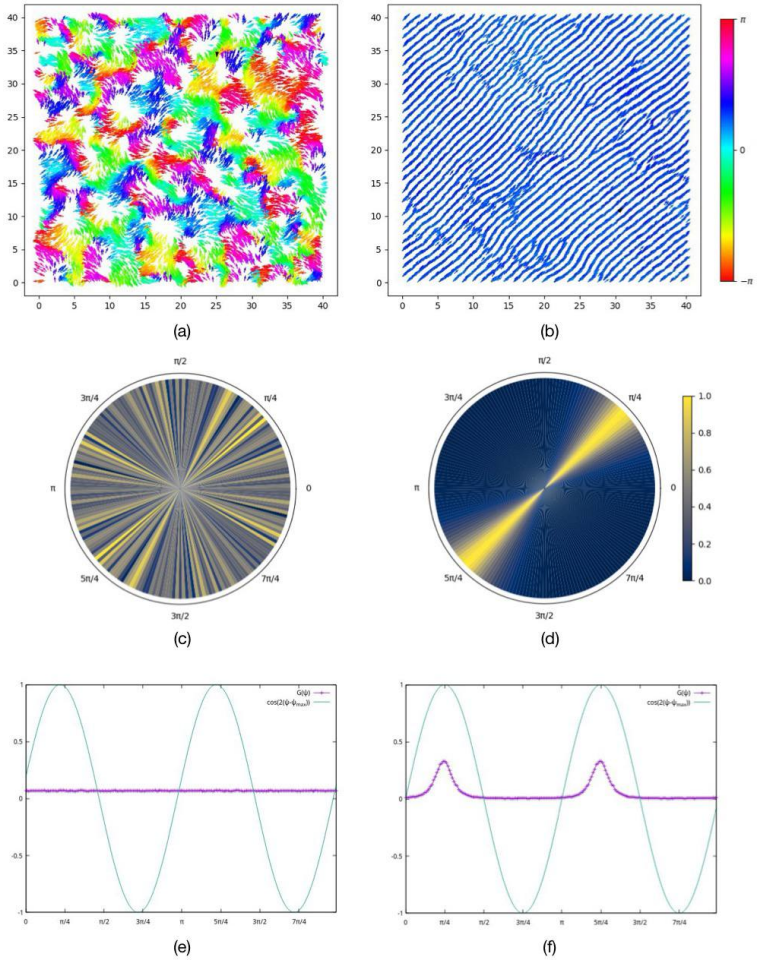

Figure 2.3: (a),(b) Snapshots of configurations right after particles have been generated from a uniform distribution(left) and after some time, when smectic order has emerged(right).(c),(d) Colormap of the angular correlation function rescaled into the interval $[0, 1]$.(e),(f) $G(\psi)$ and $\cos(2(\psi - \psi^*))$ in the same plot. The two configuration correspond respectively to $S \approx 0$ and $S \approx 0.77$.

2.3.2 Phase Diagram and Finite Size Scaling of Smectic Order

With the order parameter defined in the previous section, we are now ready to analyze smectic order more quantitatively. Our focus will be on the anisotropic model with side repulsion. As previously mentioned, smectic order emerges within the orientationally ordered phase at low noise levels and moderate repulsion strengths.

The maximum noise level at which a significant smectic order is ob-

served increases with β, as expected from the competition between order and disorder. Additionally, smectic order tends to be more stable at higher densities. This can be explained by the fact that increasing the number of particles does not alter the number of smectic layers but instead makes them denser. As a result, these layers gain a form of rigidity due to alignment interactions.

Figure 2.4 presents a portion of the (β, σ) plane, displaying the corresponding levels of smectic order. The agreement with the results in [16] confirms that S is a reliable and effective smectic order parameter.

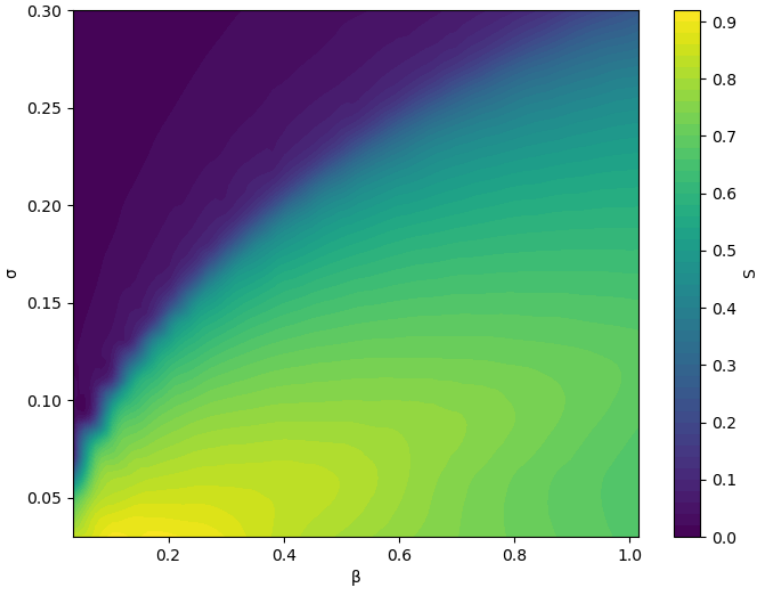

Figure 2.4: Average smectic P order parameter (S) over the (β, σ) plane, for a system of size $L = 24$.

An analysis of the system's behavior with increasing size reveals that global smectic order tends to decay beyond a certain length scale, even though it remains present locally. This suggests that the emergence of global smectic order is more likely a finite-size effect rather than a true phase.

This decay of smectic order can be understood through a phenomenological hydrodynamic theory [16]. Similar to the Toner-Tu equations discussed in the previous chapter, one can introduce a displacement field for the smectic layers and construct a symmetry-based system of partial differential equations for both this field and the density field. This theoretical framework explains the decay of smectic order in larger systems, as symmetry-allowed nonlinearities become more significant at larger scales

while remaining negligible in smaller systems.

The decay of smectic order as system size increases is illustrated in Figure 2.5, for a fixed noise level.

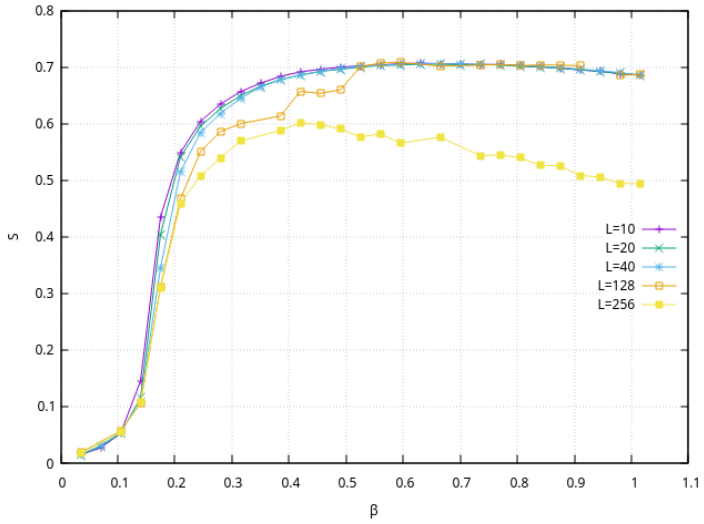

Figure 2.5: Finite size scaling for the smectic order with fixed noise ($\sigma = 0.15$). Beyond some length scale the global smectic order starts to decay.

2.4 Chiral Simmetry Breaking

In the following section, we will explore another phenomenon associated with the emergence of smectic order in the anisotropic model with $\gamma = \frac{\pi}{2}$: the onset of chirality. It has been observed that in this model, smectic configurations begin to rotate in either direction, spontaneously breaking right-left symmetry. This global rotation occurs through the breaking and reattachment of layers to neighboring ones, rather than individual particles hopping between layers. By tracking the maximum of $G(\psi)$, we can quantify the angular velocity Ω. In Figure 2.6, we present the average angular velocity of the global smectic order over an interval of $2 \cdot 10^4$, plotted as a function of the repulsion strength for different noise levels. This behavior brings up the issue of determining the nature of the transition to rotation.

By examining the dynamics of the smectic angle (Figure 2.7), it becomes evident that there is an inversion rate for the rotation, which depends on the repulsion strength. This phenomenon can also be analyzed from the perspective of the distribution of local angular velocities. By selecting a small time interval, one can compute the average angular velocity over that period, and by repeating this process, construct the histogram of the occurrences of Ω. As β increases, the behavior of the distribution becomes

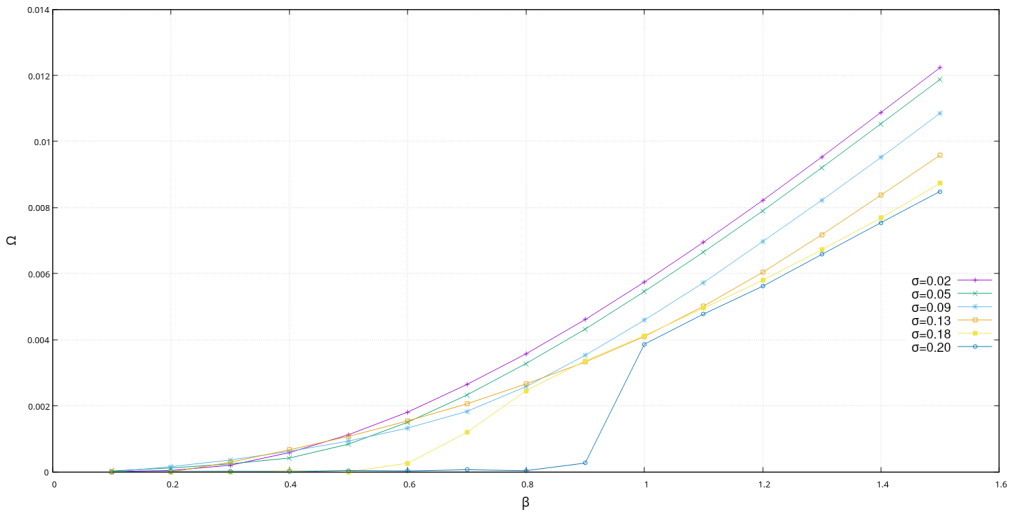

Figure 2.6: Average global angular velocity as a function of repulsion strength β, for different noise intensities. averages have been computed over an interval $\Delta t = 2 \cdot 10^4$ for a sistem of size $L = 40$.

clearer. Initially, it starts as a zero-centered, symmetric distribution. However, as β increases, the distribution splits and becomes bimodal, with two maxima that are symmetric with respect to zero. This bimodal distribution reflects that symmetry is not fully broken. If enough time is allowed, the histogram will eventually become symmetric again.

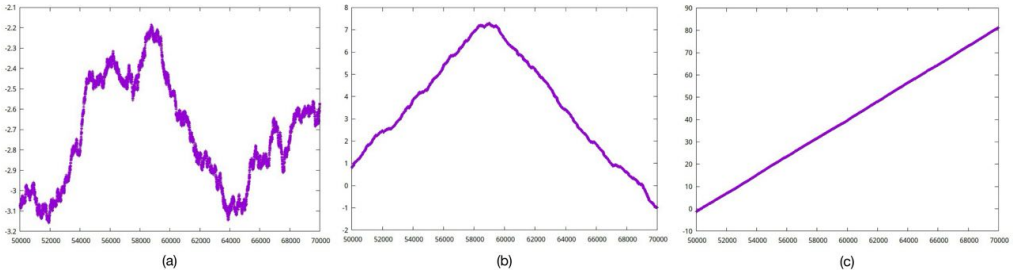

Figure 2.7: Typical smectic order angle's trajectories for increasing values of repulsion strength.

To study the mean angular velocity and its inversion rate, we can remove fluctuations in the modulus and model $\Omega(t)$ as a telegraphic process:

$$\Omega(t) = r(t)\Omega_0 \tag{2.9}$$

Where Ω_0 is a constant, and $r \in \{-1, 1\}$ is a telegraphic process with a constant rate $\lambda = \frac{1}{2\tau}$. Once the model parameters are fixed, we can evaluate Ω_0 and τ by using the autocorrelation function:

$$\langle \Omega(0)\Omega(t) \rangle = C(t) = \Omega_0^2 e^{\frac{t}{\tau}} \tag{2.10}$$

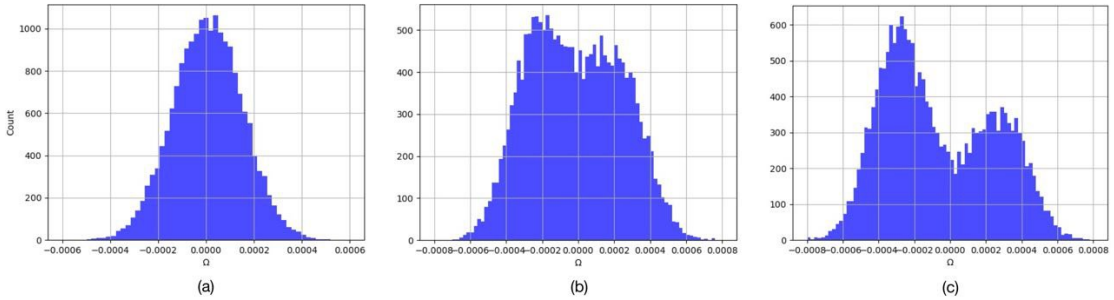

Figure 2.8: Histograms of global angular velocity computed within a time interval $\Delta t = 50$, over $T = 10^6$ time steps for a system of size $L = 40$ and for noise strength $\sigma = 0.13$.(a),(b) and (c) show the results for increasing values of β: 0.21,0.28 and 0.30, respectively.

At this point, it remains to collect sufficient data to perform an exponential fit on the autocorrelator. We are particularly interested in how this behavior varies with the repulsion strength. Some examples of the fitting results are shown in Figure 2.9 for different values of β.

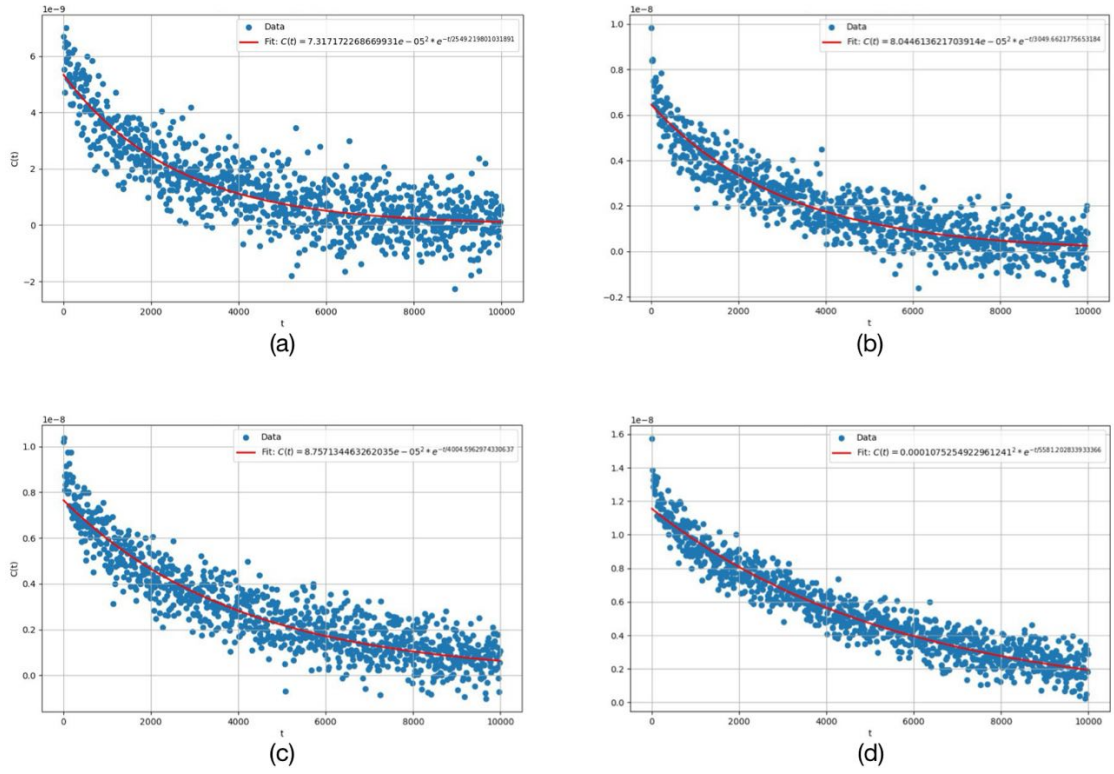

Figure 2.9: Examples of exponential fit for the angular velocity's autocorrelation function. (a),(b),(c),(d) correspond respectively to $\beta = 0.195, 0.200, 0.205, 0.215$. Averages have been computed over $2 \cdot 10^7$ time steps.

The behavior of the modulus of the angular velocity was found to be consistent with the results in Figure 2.6. The study of the rotational dynamics revealed that up to a certain level of smectic order emergence, only diffusion occurs. This explains why, in Figure 2.10, errors in τ tend to be higher for smaller values of β.

Interestingly, the inversion time τ exhibits an exponential increase with repulsion strength (Figure 2.10). While one would also expect τ to increase with system size, it should be noted that, since smectic order is a finite-size effect, there is no case of divergence. Moreover, for higher values of β the smectic order is destroyed, and rotation cannot occur. This implies that chiral symmetry is not fully broken and is, in fact, restored for timescales much larger than τ.

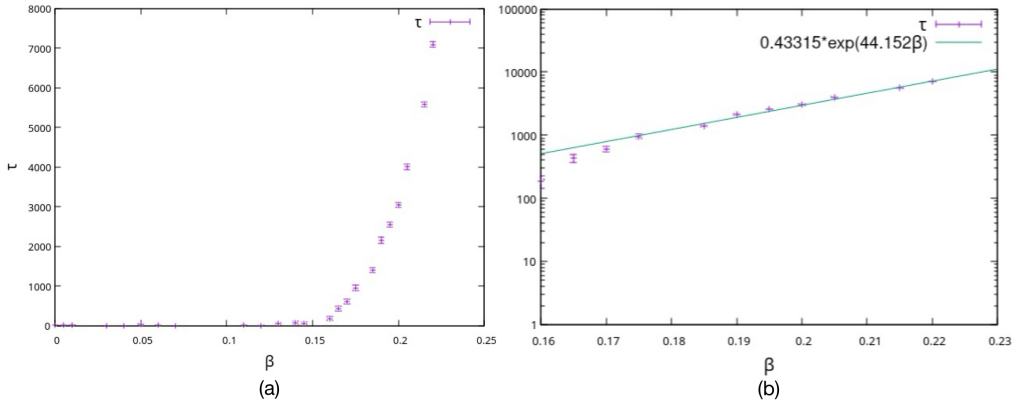

Figure 2.10: (a) Result of the exponential fit for the parameter τ. (b) Zoom on the strongly rotating regime, in logaritmic scale.

Chapter 3

Conclusions

In this thesis, we have reproduced and analyzed in detail some of the known results on Vicsek-like flocking models. The focus of this work is to inspect the role of non-reciprocal interactions in the collective dynamics of such non-equilibrium systems.

In Chapter 2, we concentrated particularly on the global rotation of smectic P configurations in the case of repulsion being stronger to the sides. We found a clear difference between isotropic and anisotropic interactions: global rotation was observed only in the latter case, despite the emergence of a new type of smectic order (type P) in both. The minimal necessary ingredients for chirality to emerge are still to be determined, and further insights must be extracted from microscopic simulations.

The next step would be to develop continuous theories derived from microscopic models, capable of accounting for chiral phases, as the current phenomenological smectic P hydrodynamic equations do not capture this behavior.

Appendix A

Active Ising Model

The Active Ising Model (AIM) [18] was introduced as an alternative approach to studying the flocking transition. It helps to overcome some of the numerical and analytical challenges posed by the Vicsek model while still capturing the essential ingredients of flocking: self-propulsion and alignment interactions. However, unlike the Vicsek model, which has continuous rotational symmetry, the AIM is based on a discrete Ising-like symmetry. In this model, particles move in a two-dimensional space but self-propulsion is restricted to only two possible directions: left or right. Despite its simplicity, the AIM reproduces much of the same physics as Vicsek-type models while being more mathematically and computationally tractable.

We consider N particles moving on a $2D$ lattice with periodic boundary conditions. Each particle carries a spin ± 1 and there are no exluded volume interactions, meaning there can be an arbitrary number of particles $n_i^{\pm}$ with spin $\pm$ on each site. The local density and magnetization are then defined as $\rho_i = n_i^+ + n_i^-$ and $m_i = n_i^+ - n_i^-$. The dynamics is determined as a continuous-time Markov process in which particles can both flip their spins and hop to neighboring lattice sites at rates that depend on their spin:

- Spin flip: represents the alignment.
  A particle with spin s on site i flips its spin at rate:

$$W(s \to -s) = \gamma \exp\left(- s\beta \frac{m_i}{\rho_i} \right) \tag{A.1}$$

  Where $\beta = \frac{1}{T}$ plays the role of inverse temperature and the rate γ can be set $\gamma = 1$ by rescaling time. This interaction is purely local: particles only interact within the same site. The flipping rate varies depending on the local magnetization: it is highest when all neighboring spins are opposite and lowest when they are aligned.

- Hopping: represents the self-propulsion.
  Particles undergo free diffusion on the lattice with a left/right bias

depending on the sign of their spins: a particle with spin s hops with rate $D(1+s\epsilon)$ to its right, $D(1-s\epsilon)$ to its left and D in both up and down directions. Thus, the parameter ϵ controls the strength of the self-propulsion.

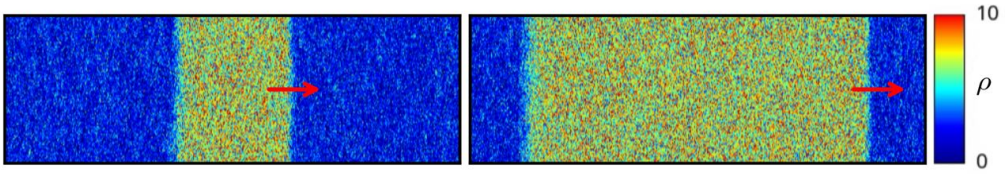

Figure A.1: Adapted from [20]. Phase separation in the active Ising model. $L_x = 800$, $L_y = 100$, $D = 1$, $\epsilon = 0.9$, $\beta = 1.9$, $\rho_1 = 2.35$(left), $\rho_2 = 4.7$(right). Red arrows indicate direction of motion.

In this model, flocking corresponds to a phase transition similar to a liquid-gas transition, where an ordered, dense liquid phase coexists with a disordered gas phase. However, unlike the Vicsek model, where flocking appears as traveling bands within a disordered background, the AIM exhibits complete phase separation: a single large, dense cluster moves as a coherent unit through a dilute gas (Figure A.1). This macroscopic phase separation has been extensively studied using both numerical simulations and mean-field theoretical approaches [19].

Appendix B

Boltzmann Equation for Polar Vicsek Particles

It is possible to develop a kinetic theory for the generalized Vicsek model through the introduction of a generalized Boltzmann equation [15]. We first define the single-particle distribution function $f(\vec{r}, \theta, t)$, connected to the probability to find a particle at position $\vec{r}$ heading in the direction specified by θ, at time t. The normalization is chosen such that:

$$\frac{1}{V}\int_V d\vec{r}\int_{-\pi}^{\pi} d\theta f(\vec{r}, \theta, t) = \rho_0$$

Where V is the total volume and ρ_0 is the mean density of the system.

Let us begin the derivation from the positional part of the master equation. The starting point involves expressing the single-particle distribution as:

$$f(\vec{r}, \theta, t) = \int d\vec{v}\phi(v, \theta_v - \theta) f(\vec{r} - \vec{v}\Delta t, \theta, t)$$

On time scales much larger than Δt we can apply Itô calculus to expand f inside the integral, leading to:

$$\partial_t f(\vec{r}, \theta, t) + \langle v_\alpha\rangle\partial_\alpha f(\vec{r}, \theta, t) = \frac{1}{2}\langle\delta v_\alpha \delta v_\beta\rangle\Delta t\partial_\alpha\partial_\beta f(\vec{r}, \theta, t)$$

Where $\langle\cdot\rangle$ denotes the average over $\phi(v, \delta\theta)$ and $\delta\vec{v} = \vec{v} - \langle\vec{v}\rangle$. Since we are considering polar particles, $\langle\vec{v}\rangle$ points in the direction defined by θ. We can then write $\langle\vec{v}\rangle = v_0\hat{n}(\theta)$, where $\hat{n}(\theta) = (\cos\theta, \sin\theta)$ and $v_0 = \langle v\cos\delta\theta\rangle$. The covariance term can be evaluated, yielding a decomposition into an isotropic term proportional to the identity $\delta_{\alpha\beta}$ and an anisotropic term proportional to the nematic tensor $q_{\alpha\beta}(\theta) = n_\alpha(\theta)n_\beta(\theta) - \frac{1}{2}\delta_{\alpha\beta}$:

$$\langle\delta v_\alpha\delta v_\beta\rangle = \frac{1}{2}\langle v^2\big(1 - \cos 2\delta\theta\big)\rangle\delta_{\alpha\beta} + \big(\langle v^2\cos 2\delta\theta\rangle - v_0^2\big)n_\alpha(\theta)n_\beta(\theta)$$

which can be rewritten as:

$$\langle \delta v_\alpha \delta v_\beta \rangle = \frac{1}{2}\big(\langle v^2 \rangle - v_0^2\big)\delta_{\alpha\beta} + \big(\langle v^2 \cos 2\delta\theta \rangle - v_0^2\big) q_{\alpha\beta}$$

Thus, the positional part of the Boltzmann equation becomes:

$$\partial_t f(\vec{r},\theta,t) + v_0 n_\alpha(\theta)\partial_\alpha f(\vec{r},\theta,t) = D_0 \Delta f(\vec{r},\theta,t) + D_1 q_{\alpha\beta}\partial_\alpha\partial_\beta f(\vec{r},\theta,t) \tag{B.1}$$

where

$$D_0 = \frac{1}{4}\big(\langle v^2 \rangle - v_0^2\big)\Delta t \tag{B.2}$$

$$D_1 = \frac{1}{2}\big(\langle v^2 \cos 2\delta\theta \rangle - v_0^2\big)\Delta t \tag{B.3}$$

are the isotropic and anisotropic diffusion constants, respectively.

To derive the full master equation, we must also consider the dynamics of the heading angle θ. This requires two main assumptions:

- Low-density regime: In this regime, the dynamics of θ are dominated by self-diffusion and binary collision events, with interactions involving more than two particles being negligible.
- Molecular chaos: This assumes that the headings of particles become uncorrelated between consecutive collisions, allowing for the factorization of the two-particle distribution function as:

$$f^{(2)}(\vec{r},\theta_1,\theta_2,t) \approx f(\vec{r},\theta_1,t) f(\vec{r},\theta_2,t). \tag{B.4}$$

Let us now analyze the two events separately.
In self-diffusion, the heading angle changes by an amount drawn from the symmetric distribution $P_\eta(\delta)$, with a standard deviation η. To incorporate the finite-time dynamics of Vicsek-like models, we include tumbling events occurring at a rate λ:

$$I_{sd}[f] = -\lambda f(\vec{r},\theta,t) + \lambda \int_0^{2\pi} d\theta' f(\vec{r},\theta',t) P_\eta(\theta - \theta') \tag{B.5}$$

In binary collisions, two particles with initial heading angles θ_1 and θ_2 have their headings updated after the collision to:

$$\theta_1' = \Psi(\theta_1,\theta_2) + \delta_1$$
$$\theta_2' = \Psi(\theta_2,\theta_1) + \delta_2$$

Where δ_1 and δ_2 are drawn from $P_\eta(\delta)$.
Since we consider polar particles, the interaction rule Ψ must be 2π-periodic.

Additionally, due to the isotropy of the model, Ψ must satisfy the following symmetry property for any rotation by an angle ϕ:

$$\Psi(\theta_1 + \phi, \theta_2 + \phi) = \Psi(\theta_1, \theta_2) + \phi \mod 2\pi$$

By choosing $\phi = -\theta_1$, we obtain:

$$\Psi(\theta_1, \theta_1 + \Delta) = \theta_1 + \Psi(0, \Delta) \tag{B.6}$$

Where $\Delta = \theta_2 - \theta_1$.
From (B.6), it follows that the interaction rule can be parameterized by $H(\Delta) \doteq \Psi(0, \Delta)$.
The collision rate can be expressed through a collision kernel $K(\Delta)$. The number of collisions per unit volume and unit time for a particle at $(\vec{r}, \theta_1)$ interacting with another particle with heading θ_2 is given by:

$$N_c = 2r_0 v_0 K(\Delta) f^{(2)}(\vec{r}, \theta_1, \theta_2, t)$$

where r_0 is the interaction radius. Using the molecular chaos assumption, we substitute the factorized form of $f^{(2)}$ from (B.4). The collision contribution then becomes:

$$\begin{aligned} I_{col}[f] = &-2r_0 v_0 f(\vec{r}, \theta, t) \int_0^{2\pi} d\theta' K(\theta' - \theta) f(\vec{r}, \theta, t) + \\ &+ 2r_0 v_0 \int_0^{2\pi} d\theta_1 \int_0^{2\pi} d\theta_2 K(\theta_2 - \theta_1) f(\vec{r}, \theta_1, t) f(\vec{r}, \theta_2, t) P_\eta\big(\theta - \Psi(\theta_1, \theta_2)\big) \end{aligned} \tag{B.7}$$

Combining the heading dynamics contributions from (B.5) and (B.7) with the positional part of the Boltzmann equation (B.1), we arrive at the full master equation:

$$\begin{aligned} \partial_t f(\vec{r}, \theta, t) + v_0 n_\alpha(\theta) \partial_\alpha f(\vec{r}, \theta, t) = D_0 \Delta f(\vec{r}, \theta, t) + D_1 q_{\alpha\beta} \partial_\alpha \partial_\beta f(\vec{r}, \theta, t) + \\ + I_{sd}[f] + I_{col}[f] \end{aligned} \tag{B.8}$$

Finally, we must specify the functional forms of the collision kernel $K(\Delta)$ and the interaction rule $H(\Delta)$. For the scenario of interest, the kernel takes the form:

$$K(\theta_2 - \theta_1) = |\hat{n}(\theta_2) - \hat{n}(\theta_1)| = 2\left|\sin\left(\frac{\Delta}{2}\right)\right| \tag{B.9}$$

while the interaction rule, in the canonical Vicsek model corresponds to:

$$H(\Delta) = \frac{\Delta}{2} \quad \forall \Delta \in (-\pi, \pi] \tag{B.10}$$

Bibliography

[1] Bartolo D. Bain N. Dynamic response and hydrodynamics of polarized crowds. *Science*, 363:46–49, 2019.

[2] M. Ballerini, N. Cabibbo, R. Candelier, A. Cavagna, E. Cisbani, I. Giardina, V. Lecomte, A. Orlandi, G. Parisi, A. Procaccini, M. Viale, and V. Zdravkovic. Interaction ruling animal collective behavior depends on topological rather than metric distance: Evidence from a field study. *Proceedings of the National Academy of Sciences*, 105(4):1232–1237, 2008.

[3] Eric Bertin, Michel Droz, and Guillaume Grégoire. Boltzmann and hydrodynamic description for self-propelled particles. *Phys. Rev. E*, 74:022101, Aug 2006.

[4] Ivo Buttinoni, Julian Bialké, Felix Kümmel, Hartmut Löwen, Clemens Bechinger, and Thomas Speck. Dynamical clustering and phase separation in suspensions of self-propelled colloidal particles. *Phys. Rev. Lett.*, 110:238301, Jun 2013.

[5] Michael E. Cates and Julien Tailleur. Motility-induced phase separation. *Annual Review of Condensed Matter Physics*, 6(Volume 6, 2015):219–244, 2015.

[6] Hugues Chaté, Francesco Ginelli, Guillaume Grégoire, and Franck Raynaud. Collective motion of self-propelled particles interacting without cohesion. *Phys. Rev. E*, 77:046113, Apr 2008.

[7] Hugues Chaté. Dry aligning dilute active matter. *Annual Review of Condensed Matter Physics*, 11(Volume 11, 2020):189–212, 2020.

[8] Qiu-shi Chen, Aurelio Patelli, Hugues Chaté, Yu-qiang Ma, and Xiaqing Shi. Fore-aft asymmetric flocking. *Phys. Rev. E*, 96:020601, Aug 2017.

[9] András Czirók, H Eugene Stanley, and Tamás Vicsek. Spontaneously ordered motion of self-propelled particles. *Journal of Physics A: Mathematical and General*, 30(5):1375, mar 1997.

[10] Guillaume Grégoire and Hugues Chaté. Onset of collective and cohesive motion. *Phys. Rev. Lett.*, 92:025702, Jan 2004.

[11] Dirk Helbing, Illés Farkas, and Tamás Vicsek. Simulating dynamical features of escape panic. *Nature*, 407:487–490, 2000.

[12] Mauro Mobilia, Ivan T. Georgiev, and Uwe C. Täuber. Phase transitions and spatio-temporal fluctuations in stochastic lattice lotka–volterra models. *Journal of Statistical Physics*, 128:447–483, 2007.

[13] Steinberg AP Pine DJ Chaikin PM Palacci J, Sacanna S. Living crystals of light-activated colloidal surfers. *Science*.

[14] Matteo Paoluzzi, Marco Leoni, and M. Cristina Marchetti. Information and motility exchange in collectives of active particles. *Soft Matter*, 16:6317–6327, 2020.

[15] A. Peshkov, E. Bertin, F. Ginelli, and H. Chaté. Boltzmann-ginzburg-landau approach for continuous descriptions of generic vicsek-like models. *The European Physical Journal Special Topics*, 223, 2014.

[16] Pawel Romanczuk, Hugues Chaté, Leiming Chen, Sandrine Ngo, and John Toner. Emergent smectic order in simple active particle models. *New Journal of Physics*, 18(6):063015, jun 2016.

[17] Semmrich C Frey E Bausch AR Schaller V, Weber C. Polar patterns of driven filaments. *Nature*.

[18] A. P. Solon and J. Tailleur. Revisiting the flocking transition using active spins. *Phys. Rev. Lett.*, 111:078101, Aug 2013.

[19] A. P. Solon and J. Tailleur. Flocking with discrete symmetry: The two-dimensional active ising model. *Phys. Rev. E*, 92:042119, Oct 2015.

[20] Alexandre P. Solon, Hugues Chaté, and Julien Tailleur. From phase to microphase separation in flocking models: The essential role of nonequilibrium fluctuations. *Phys. Rev. Lett.*, 114:068101, Feb 2015.

[21] Shitaka Y Tanaka D Yoshikawa K Chaté H Oiwa K. Sumino Y, Nagai KH. Large-scale vortex lattice emerging from collectively moving microtubules. *Nature*.

[22] I. Theurkauff, C. Cottin-Bizonne, J. Palacci, C. Ybert, and L. Bocquet. Dynamic clustering in active colloidal suspensions with chemical signaling. *Phys. Rev. Lett.*, 108:268303, Jun 2012.

[23] John Toner and Yuhai Tu. Long-range order in a two-dimensional dynamical XY model: How birds fly together. *Phys. Rev. Lett.*, 75:4326–4329, Dec 1995.

[24] Tamás Vicsek, András Czirók, Eshel Ben-Jacob, Inon Cohen, and Ofer Shochet. Novel type of phase transition in a system of self-driven particles. *Phys. Rev. Lett.*, 75:1226–1229, Aug 1995.

[25] Christos C Ioannou Cristián Huepe Iain D Couzin Yael Katz, Kolbjørn Tunstrøm. Inferring the structure and dynamics of interactions in schooling fish. *Proc. Natl. Acad. Sci. USA*.